Korean J. Chem. Eng., **27**(1), 83-90 (2010)
DOI: 10.2478/s11814-009-0297-1

A study on vortex generators to improve the mixing rate in the dry sorbent injection process of the flue gas desulfurization system

Jin Do Chung*,†, Jang Woo Kim, and Young Moon Park*****

*Department of Environmental Engineering, Hoseo University, Asan 336-795, Korea
**Department of Display Engineering, Hoseo University, Asan 336-795, Korea
***Department of Semiconductor & Display Engineering, Graduate School, Hoseo University, Asan 336-795, Korea
(*Received 4 July 2007 • accepted 3 June 2009*)

Abstract−The aim of this study is to improve mixing rate of dry sorbent injection technology (DSI). A CFD (Computational Fluid Dynamics) code is used to predict the sorbent dispersion rate, pressure drop and turbulent kinetic energy of mixing particles and gas flow for three different vortex generators, which have been designed for the inside of the duct. After analyzing simulated results, it was shown that a similar trend of change in the dispersion rate in three different vortex generators had taken place and that the dispersion rate curve could reach over 80% by applying the lobed-plate and guide-vane(B) vortex generators. The lowest pressure drop was obtained when a lobed-plate was installed, whereas the highest pressure drop occurred when a guide-vane(A) was installed. The turbulent kinetic energy is nearly always stable when a lobed-plate is applied, but increases very quickly after passing through a guide-vane and then slowly decreases when a guide-vane(B) is applied. The situation for in the case of guide-vane(A) is somewhat more complicated.

Key words: Dry Sorbent Injection (DSI), Vortex Generator, Gas-solid Flow, Sorbent Dispersion

INTRODUCTION

Thermal power plants have been increasing in number as the need for electricity has grown. This has led to an increase in the amount of coal being used. The extraordinary rate of development of the power industry in the Korea over the past few decades has brought not only a growing concern with regard to environmental issues here, but has also caused economists around the world to re-think what the environmental consequences will be if the forecasted explosive growth in economic activity takes place elsewhere around the world. The need to control SO_2 emissions has been recognized as an important factor that will help develop industry here and contribute to the further modernization of Korea in a way that minimizes the negative impact both on the health of the population and on the environment. Reducing SO_2 emission from power plants is a key issue for environmental protection [1]. Several FGD (Flue Gas Desulfurization) technologies have been developed recently in a number of countries. The research and development have progressed to the point where an array of processes is available to cover a broad range of site-specific, technical, economic situations [2].

In an effort to limit the SO_2 emissions of South Korea coal power plants to a degree allowed by current air pollutant standards, DSI technology, which is one of the FGD technologies that has been adapted between the preheater and particulate collector in the technological assembly line, is a very attractive option. It has several advantages such as low capital and operational costs, the simplicity of the process and its adaptability to difficult retrofit situations, and there being no need for a waste water treatment plan [3]. However, the DSI process entails the injection of dry sorbent into the ductwork, so the technology to disperse sorbent in a uniform way is urgently required. In this study, the method of attaining this uniform dispersion of sorbent was attained by mixing the gas-sorbent phase.

To provide rapid mixing, streamwise vorticity can be introduced into the flowing streams by other means: for example, by installing three different vortex generators immediately downstream of the wavy trailing edge or with a triangular shaped prism [4].

Splitter plates with a convoluted wavy trailing edge are commonly referred to as "lobed forced mixers." The geometry of the lobe causes large-scale, streamwise vorticity to be shed at the trailing edge. The enhanced mixing characteristics of the lobed mixers are directly attributable to the large mixing scales generated by the streamwise vorticity. Also, guide-vanes shaped in the manner of a triangular prism can enhance mixing characteristics inside duct work [5].

This present study includes experimental data of the three different vortex generators that were analyzed to assess their characteristics and to ascertain the pressure drop in the fluid flow field in the duct. However, this approach is quite expensive and a long time may elapse before significant experimental results are known.

The numerical prediction of dilute particulate flows in a duct has a wide range of engineering applications that can be performed using a CFD code to model gas-solid flows that have a different cross-section geometry and flow orientation. For the gas phase, local mean gas flow properties, such as velocity and kinetic energy, are calculated numerically by solving a set of Reynolds-averaged Navier-Stokes partial differential equations using a CFD code. For the solid phase, instantaneous positions and velocities of the dispersed phase are solved from a set of ordinary differential equations in accordance with a Lagrangian particle tracking methodology [6].

†To whom correspondence should be addressed.
E-mail: jdchung@hoseo.edu

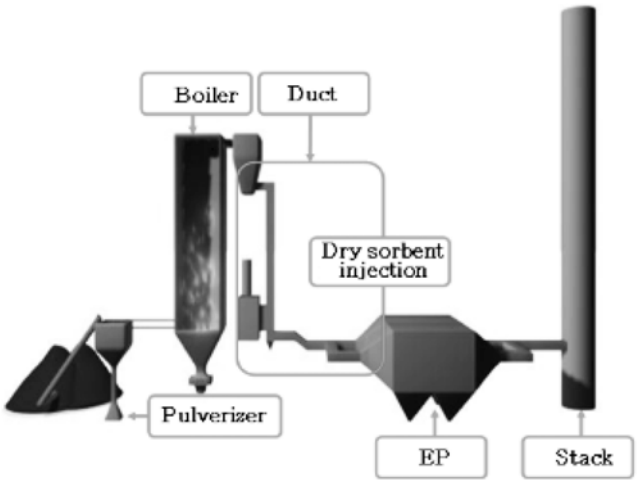

Fig. 1. Schematic diagram of the thermal power plant.

Table 1. Specification of vortex generators

Items	Design factor (m)			Quantity	Shape
Lobed-plate	W	7.4		1	
	H	3			
	L	3			
Guide-vane(A)	W	3.7 7.4	2 type	4	
	H	1			
	L	2			
Guide-vane(B)	W	3.7 7.4	2 type	4	
	H	1			
	L	1			

In the case of DSI, the applications of CFD modeling can be focused on studying the $Ca(OH)_2$ injection into the ductwork including finding the duct structure for creating a uniform dispersion during the solid phase into the flue gas stream.

MATERIAL AND METHODS

1. Air-particle Mixing Approaches

It has been established that this technology consists of the injection of dry sorbent into the ductwork downstream between the boiler and the particulate collector. Thus, the ductwork shapes and structural designs are very important before any numerical calculation is performed. Ductwork structure introduces particle dispersion and a fluid flow field that affect the efficiency of the reaction between $Ca(OH)_2$ and SO_2 and also the efficiency of the SO_2 removal process [7]. As the gas-solid mixing approaches the duct, a double vortex flow structure occurs in the fluid phase. Both the momentum of particles and the velocity of gas are associated with the particulate loading and Stokes number. The first step in solving any multiphase problem is to determine which state is more clearly represented [8].

A uniform dispersion of sorbent across the duct and adequate

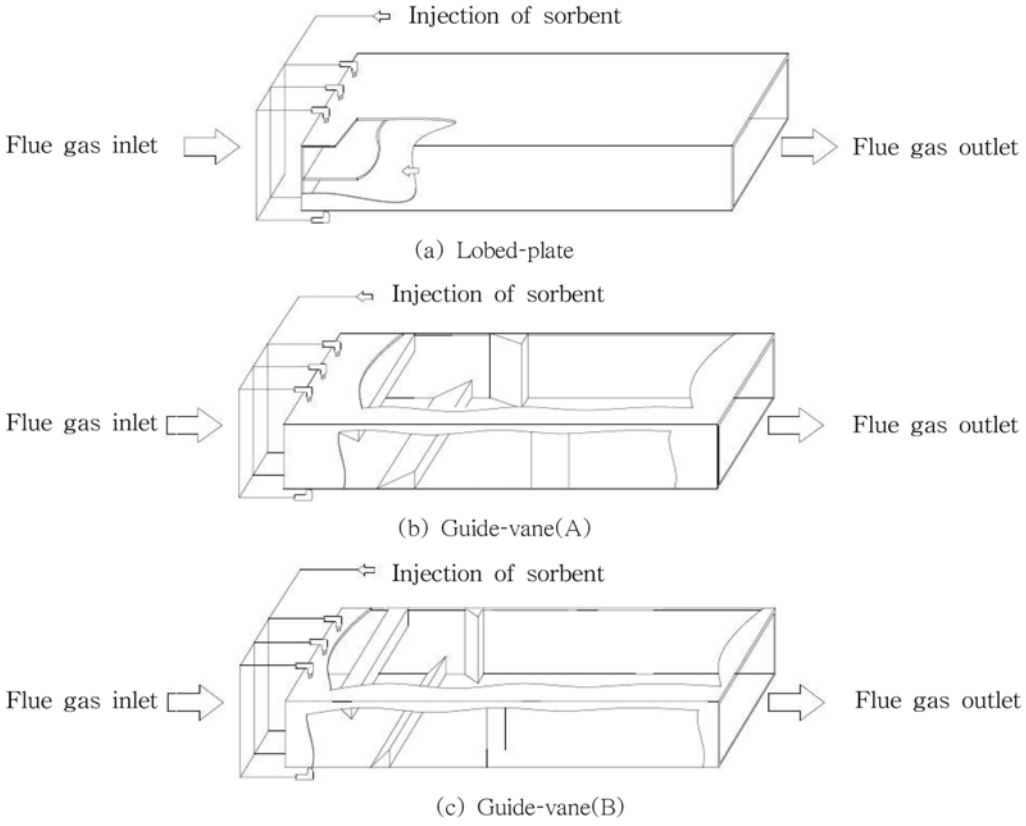

Fig. 2. Shapes of the duct structure.

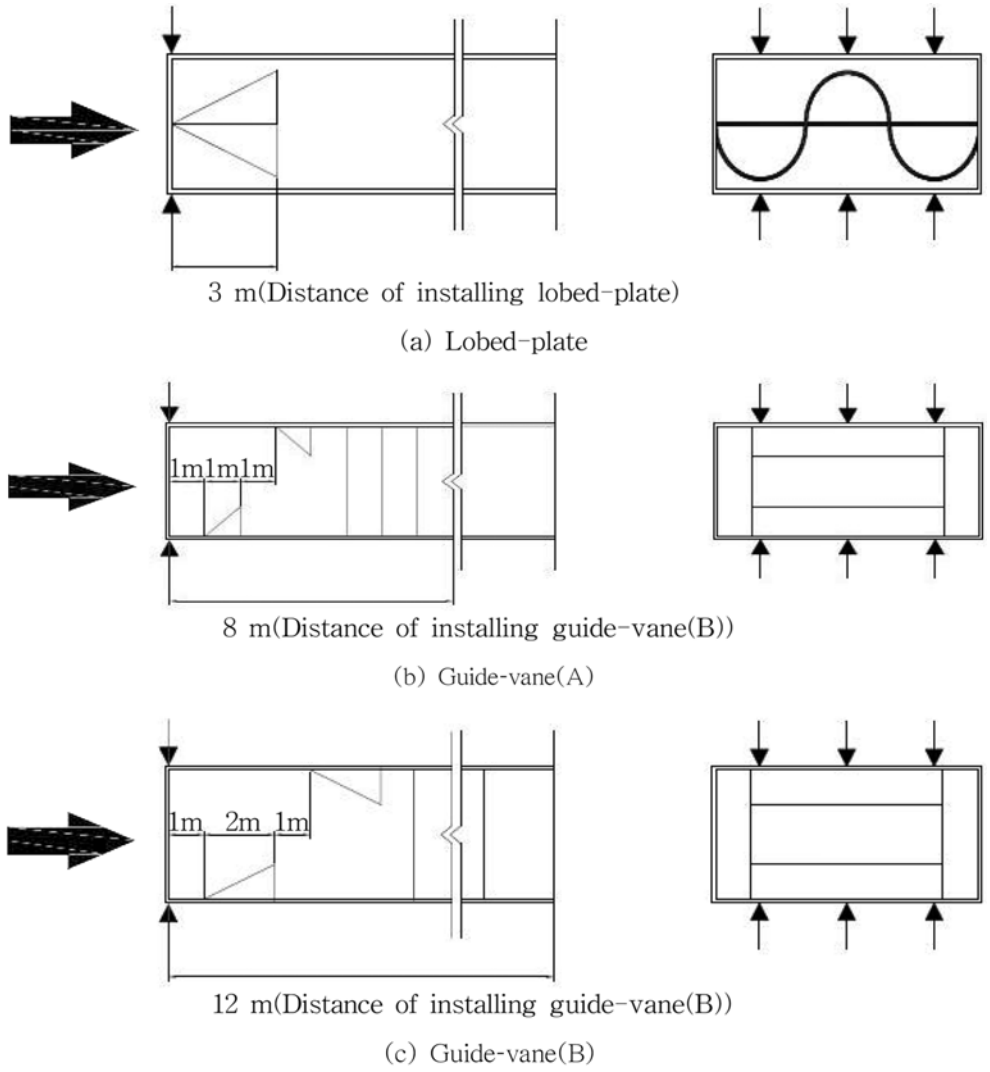

Fig. 3. Description regarding the injection position of sorbent and the distance of installed vortex generators.

residence time are critical for high SO_2 removal rates. The sorbent is dispersed uniformly as soon as the injection of sorbent into the fluid flow field occurs in the duct [9].

The change in the fluid flow field is induced through structural design of the duct. It can affect to sorbent dispersion. For this reason the present study did numerical analysis on the three different vortex generators to evaluate the effectiveness of sorbent dispersion. Table 1 and Fig. 2 show the specifications of the vortex generators (1) lobed-plate, (2) guide-vane(A), (3) guide-vane(B).

The application of lobed-plate and guide-vanes is considered when designing the duct structure as vortex generators. They are two useful ways to enhance the mixing of particles and flue gas.

When the lobed-plate was installed inside the duct at the inlet position, an examination was performed that determined the height, length, and width as 3 m; 3 m and 7.4 m, respectively. In the other cases, four guide-vanes were installed on the walls of duct. In still other cases, two types of guide-vanes (A and B) were installed and the measurements were as follows: height, length, and width as 1 m; 2 m and 3.7 m or 7.4 m for guide-vane A and 1 m; 1 m and 3.7 m or 7.4 m for guide-vane B, respectively.

The fluid medium is air, and is passed through three different vortex generators with mesh structures prior to entering the test duct. The duct width, height, and length are 7.4 m, 3.7 m and 23 m, respectively. A detailed 2-dimensional description with the dimensions of the vortex generators is shown in Fig. 3.

To ensure effective sorbent distribution in flue gas flow, not only is the application of vortex generators needed but also injection nozzles are required. A set of six injection nozzles, which was divided into two groups, was designed for the shape of the duct walls. These nozzles - indicated by the arrows (↓, ↑) - are connected to an air compressor to supply $Ca(OH)_2$ with 1.2 kg/s.

COMPUTATIONAL MODELING AND PROCEDURE

In the study of the flue gas flow and particle dispersion along the duct, based on design data, there is a step-by-step approach that covers three basic areas: (a) geometry, (b) grid generation and (c) flow simulation.

1. Geometry

The positions of the injection nozzles, the vortex generators and

Table 2. Specification of grid generation

Items	The number of nodes	Ducts
Lobed-plate	157495	
Guide-vane(A)	287420	
Guide-vane(B)	125118	

the duct structure, which have been described in the above section, have been checked for dimensional accuracies. The inlet/outlet of flue gas flow has been also determined.

2. Grid Generation

The vortex generators, ducts and domains are modeled and meshed by using a commercial software package, Gambit 2.1. Table 2 shows the surface meshes for each different case. Structured hexahedron cells are attractive in creating high accuracy simulations as they can be generated for complicated geometries, typically vortex generators, without creating highly skewed cells. This is important when the goal of the study is to determine the shapes of the best vortex generators for a practical application. It was also noted that the cells are quite coarse in the boundary layer and cannot physically resolve the flow near the boundary; thus, it depends upon standard wall functions incorporated into the mathematical model to approximate the viscous sub layer.

Often, the calculation domain has a shape that does not lend itself to the subdivision of a single structured mesh. The structured grid data generated from the Gambit files exported in Fluent are shown in Table 3. They have been converted into structured grid blocks. With regard to the grid interfaces and boundary conditions, grid points are comprised for each different case. The higher grid size, with the required fineness positioned towards the wall in order to capture boundary losses, limits the hardware resources in terms of main memory, which not only makes it difficult to read the grid data but also signals insufficient memory errors in the pre-processing stage [10].

3. Boundary Condition

Specific modeling assumptions are made to set the initial and boundary conditions in the present numerical simulation. The vortex generators mixing flows are assumed incompressible, based on maximum experimental velocities recorded at 47 m/s in the ductwork. The incoming velocity in the rectangular duct flowing downstream into the vortex generators is calculated by applying the mass conservation of exit velocity. For the purposes of the present study, the inlet velocity of gas was set at a constant 17 m/s, and the inlet velocity of nozzles set at 5.1 m/s. Constant static pressure was maintained across the outlet domain extents and a boundary condition of the order of −10.24 pa was imposed.

4. Solver

The differential governing equations have indicated that all the dependent variables of interest here seem to obey a generalized conservation principle. If the dependent variable is denoted by, the general differential equation is

$$\frac{\partial(\rho\phi)}{\partial t}+\nabla(\rho\vec{u}\phi)=\nabla\cdot(\Gamma\nabla\phi)+S_{\phi} \quad (1)$$

Where, Γ is the diffusion coefficient, and S is the source term. The quantities Γ and S are specific to a particular meaning of ϕ. The dependent variable can stand for velocity components (u, v, w), pressure component (P), turbulent kinetic energy (k). Table 3 shows diffusion coefficients and term expressions for 3-D rectangular coordinate.

The continuum calculation domain has been discretized. It is this systematic discretization of space and of the dependent variables that makes it possible to replace the governing differential equations with simple algebraic equations. The procedure that we are developing for the calculation of the flow field has been given the name SIMPLE, which stands for semi-implicit method for pressure-linked equation.

The numerical predictions described in this study were performed using the Lagrangian approach provided by fluent. The numerical calculations for the gas phase were performed by solving a set of time-averaged Navier-stokes equations together with the RNG κ-ε turbulence model. The particles are introduced at a finite number of starting locations. In every given time step, their positions and velocities are calculated according to the forces acting on the particle and using Newton's second law.

In the present study, a first-order upwind scheme has been applied

Table 3. Diffusion coefficient and term expression for 3-D rectangular coordinate[11)]

Name	ϕ	Γ_{ϕ}	S_{ϕ}
x velocity	$\bar{u}$	μ_{eff}	$\frac{\partial}{\partial x}\left(\mu_{eff}\frac{\partial\bar{u}}{\partial x}\right)+\frac{\partial}{\partial y}\left(\mu_{eff}\frac{\partial\bar{v}}{\partial x}\right)+\frac{\partial}{\partial z}\left(\mu_{eff}\frac{\partial\bar{w}}{\partial x}\right)-\frac{\partial\bar{p}}{\partial x}$
y velocity	$\bar{v}$	μ_{eff}	$\frac{\partial}{\partial x}\left(\mu_{eff}\frac{\partial\bar{u}}{\partial y}\right)+\frac{\partial}{\partial y}\left(\mu_{eff}\frac{\partial\bar{v}}{\partial y}\right)+\frac{\partial}{\partial z}\left(\mu_{eff}\frac{\partial\bar{w}}{\partial y}\right)-\frac{\partial\bar{p}}{\partial y}$
z velocity	$\bar{w}$	μ_{eff}	$\frac{\partial}{\partial x}\left(\mu_{eff}\frac{\partial\bar{u}}{\partial z}\right)+\frac{\partial}{\partial y}\left(\mu_{eff}\frac{\partial\bar{v}}{\partial z}\right)+\frac{\partial}{\partial z}\left(\mu_{eff}\frac{\partial\bar{w}}{\partial z}\right)-\frac{\partial\bar{p}}{\partial z}$
Turbulent kinetic energy	κ	$\frac{\mu_{eff}}{\delta_k}$	$G_{k1}-\rho\varepsilon$
Dissipation rate of κ	ε	$\frac{\mu_{eff}}{\delta_{\varepsilon}}$	$\frac{\varepsilon}{\kappa}(C_1G_{\kappa 1}-C_2\rho\varepsilon)$

$$G\partial_{k1}=2\mu_l\left[\left(\frac{\partial\bar{u}}{\partial x}\right)^2+\left(\frac{\partial\bar{v}}{\partial y}\right)^2+\left(\frac{\partial\bar{w}}{\partial z}\right)^2\right]+\mu_l\left[\left(\frac{\partial\bar{u}}{\partial y}+\frac{\partial\bar{v}}{\partial x}\right)^2+\left(\frac{\partial\bar{v}}{\partial z}+\frac{\partial\bar{w}}{\partial y}\right)^2+\left(\frac{\partial\bar{w}}{\partial x}+\frac{\partial\bar{u}}{\partial z}\right)^2\right]$$

for all numerical simulations. Quantities at cell faces are determined by assuming that the cell-center values of any field variable represent a cell-average value and hold throughout the entire cell; the face quantities are identical to the cell quantities. Thus, the face value f is set equal to the cell-center value of the upstream cell. Fluent CFD code was used for the calculations [12].

RESULTS

The results of the numerical simulations with RNG κ-ε turbulence models are shown in Figs. 5-8 with respect to sorbent dispersion, pressure drop and turbulent kinetic energy distributions. We created the central-line and cross-sections shown in the Fig. 4 to compare the different cases. The maximum dispersion rate, pressure drop occurring by streamwise vorticity and averaged turbulent kinetic energy are plotted versus downstream distance and used to evaluate the effect of three different vortex generators on predicting the measured quantities.

1. Sorbent Dispersion

Generally, when applying DSI technology, the uniform dispersion of sorbent causes the effective and efficient removal of SO_2. With regard to this study, the gas stream passing through the ductwork was as fast as 17 m/s. This requires that the sorbent should be dispersed rapidly to achieve a high rate of SO_2 removal efficiency.

From the mean streamwise vorticity distributions shown in Table 4, it can be seen that the numerical simulations converge in revealing the evolution of sorbent dispersion generated by the special geometry of vortex generators. The "signature" of the vortex generators is evident by the streamwise vortices that correspond to three different edges of the vortex generators. A comparison of sorbent dispersion is performed at cross-sections along the duct at intervals of 5 m. The sorbent is indicated in each surface over 10-6 as volume fraction.

Table 4 exhibits the contour plots for the volume fraction of particles and predicted particle distribution rate for each different case with respect to the three different vortex generators.

To compare the particle dispersion characteristics in each case, numerical calculations were performed for all of the cases with the same conditions applied and the results analyzed by numerical prediction as in the counted area.

$$V_f = \frac{A_c}{A_t} \times 100$$

V_f: Volume fraction of sorbent in the cross-section
A_c: Counted area of sorbent in the cross-section
A_t: Counted total area of the cross-section

In the duct, the dispersion rate increases very quickly and reaches a maximum value of around 15 m. Then it slowly decreases throughout the duct. In the case of the installed guide-vane(B), the decreasing rate of sorbent dispersion in the ductwork shows signs of slowing down better than other vortex generators. In the case where the lobed-plate was installed, sorbent dispersion was achieved in the shortest time among the vortex generators considered in this study.

2. Pressure Drop

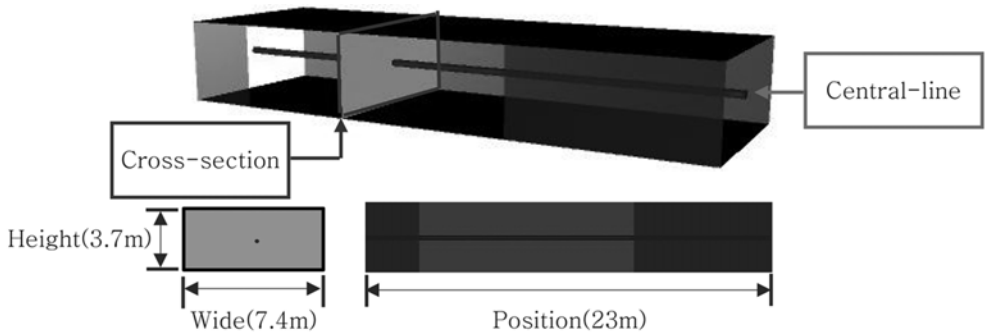

Fig. 4. Description on the central line and cross-section.

Table 4. Comparison of sorbent dispersion at each different position with respect to the vortex generators

Items	Position of observation (m)					Volume fraction of sorbent
	5	10	15	20	23	
Lobed-plate						
Guide-vane(A)						
Guide-vane(B)						

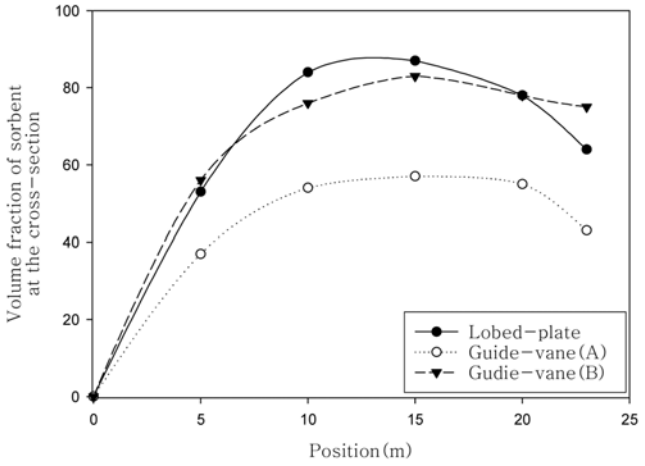

Fig. 5. Volume fraction rate of sorbent with respect to the three different vortex generators at the cross-sections of the duct.

Flow can occur in complicated geometries in various engineering devices such as the piping systems of industrial plants. Generation of streamwise vorticity or secondary motion makes the flow in the duct structure complicated and causes a larger pressure drop in the duct. The numerical simulations reveal the pressure drop in a detailed schema of data, and these results must be analyzed carefully to understand the complicated geometries involved. By observing the variation of flow properties for the three different vortex generators, it was found that the pressure drop was associated with a strong swirling motion, high velocity gradients, and shear flow at the entrance. Data obtained from the three different vortex generators are plotted in Fig. 6.

The smallest change in pressure and the lowest pressure drop are achieved when a lobed-plate vortex generator is installed at the entrance of the duct. In contrast, both the change in pressure and the pressure drop in the case when a guide-vane(B) is installed are quite noticeable. In the case where a guide-vane(A) is applied, its effect is negligible at the entrance section, but has a significant effect at the end-section of the duct. The reason for the pressure drop can be explained through a numerical analysis of the velocity vectors. Fig. 7 shows the variation of the axial velocity vectors along the duct's axis. When the gas flow goes into the duct, some pressure is lost through the force of fiction on the surface of lobed-plate or guide-vanes. After that, a convoluted shear-layer is created at the downstream position of the mixer plate. Breaking down the convoluted shear-layer gives a higher mixing efficiency and also dissipates some pressure.

3. Turbulent Kinetic Energy

Fig. 8 shows the results of the numerical simulation for the changes

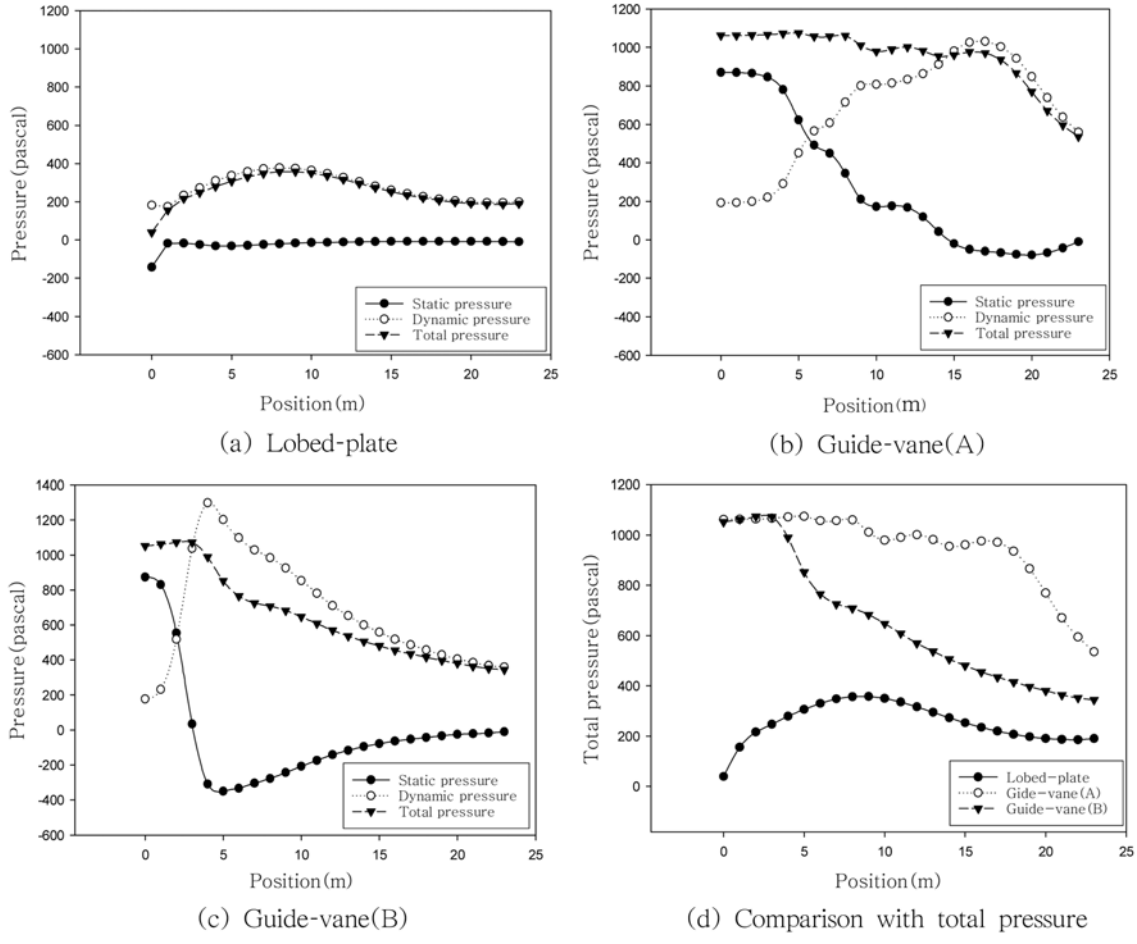

Fig. 6. Comparisons of pressure with respect to the three different vortex generators at the central line of the ductwork.

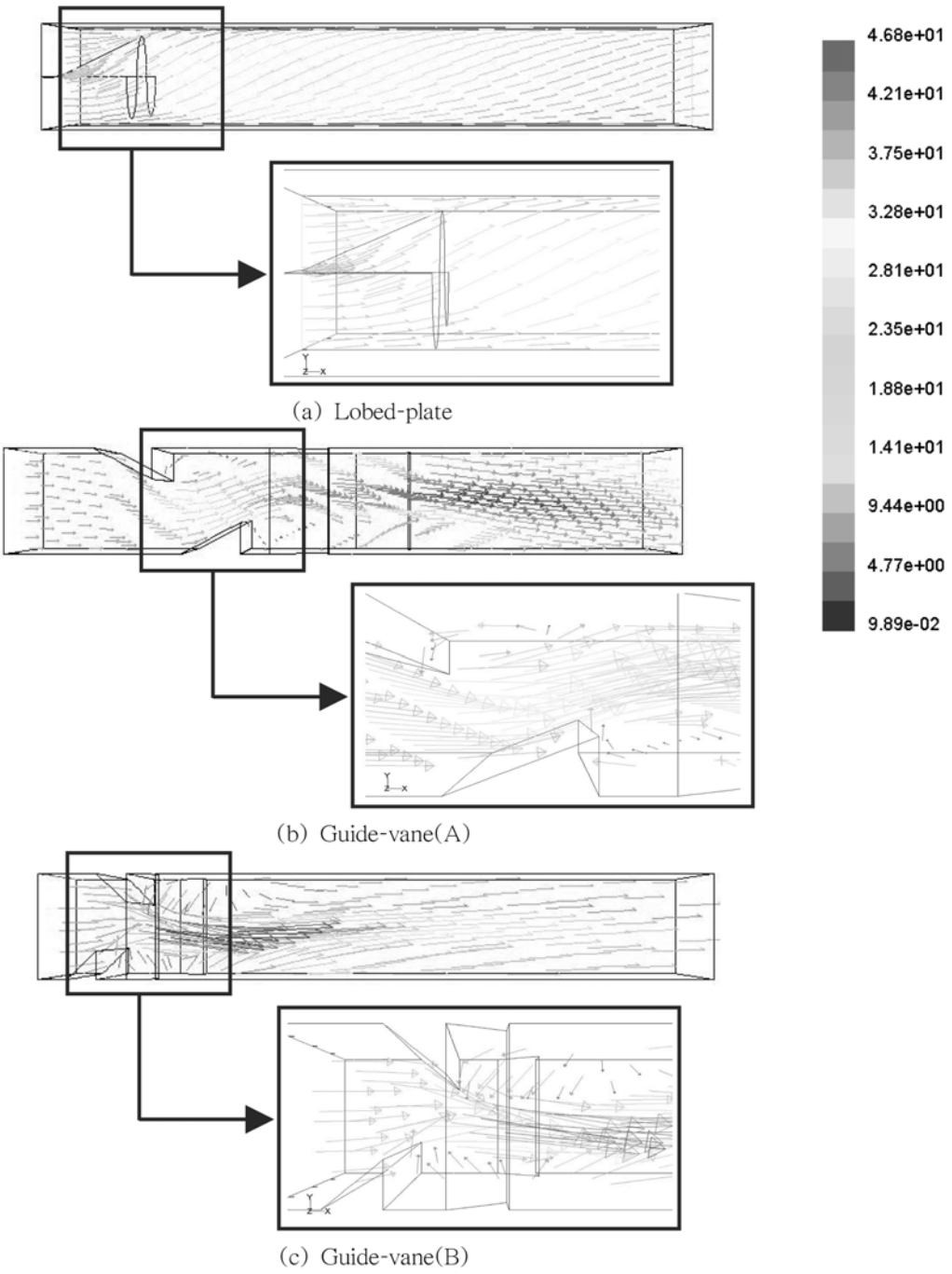

Fig. 7. Comparisons of velocity vectors for each different vortex generator.

in turbulent kinetic energy. In the case where the lobed-plate is applied, turbulent kinetic energy is almost stable. Although the streamwise vortices dissipate at downstream locations, the maximum vorticity in the vortex cell appears unchanged, and the vortex cell structure remains unaltered and uniform far downstream.

In the case where the guide-vane(A) is applied, the change in turbulent kinetic energy is small in the first part of the duct but becomes complicated at the end-part of the duct. This indicates that turbulent kinetic energy distribution at the center line of the duct is unstable, and that particle and gas flow mixing is ineffective.

In the case where the guide-vane(B) is applied, the turbulent kinetic energy increases very quickly after passing through the guide-vane and then slowly decreases. This indicates that the vorticity quickly achieves its maximum value, but because of the dissipation of turbulent kinetic energy, the vorticity slowly subsides in the remaining part.

CONCLUSIONS

To improve the SO_2 removal efficiency of dry sorbent injection technology, three different vortex generators were designed and placed inside of the duct to consider the effect on the mixing of particles

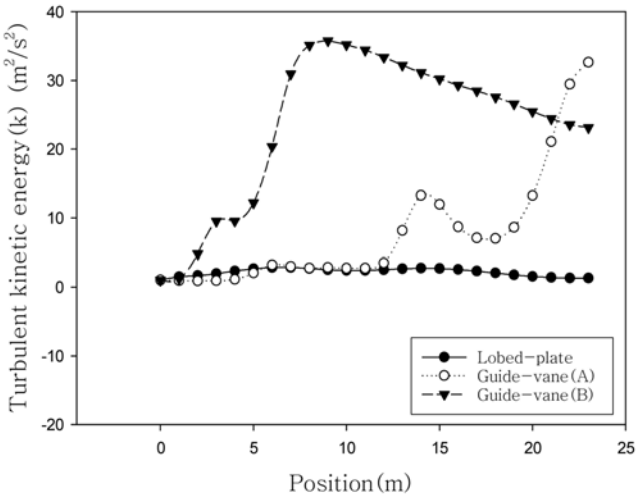

Fig. 8. Comparison of the turbulent kinetic energy with respect to the three different vortex generators at the central line of the ductwork.

and gas flow. A numerical simulation method was used to predict several properties of the flow passing through the duct. This solved a set of time-averaged Navier-Stokes equations together with the RNG κ-ε turbulence model for the gas phase. The particle position and velocity were calculated according to the forces acting on the particle and using Newton's second law for solid phases. The results were analyzed and showed the trends regarding changes in the dispersion rate in three different vortex generators were similar and the peak in the curve rate for dispersion was over 80%, achieved when applying the lobed-plate and guide-vane (B) vortex generators. The lowest pressure drop obtained resulted from the installation of the lobed-plate, whereas the highest pressure drop occurred in the case where the guide-vane (B) was installed. The turbulent kinetic energy was almost stable in the case of lobed-plate, but increased very fast initially after passing through the guide-vane and then slowly decreased in the case of guide-vane (B). The behavior of turbulent kinetic energy is more complicated in the case of guide-vane (A).

ACKNOWLEDGMENT

The authors would like to acknowledge the financial support given by the Ministry of Commerce, Industry and Energy, and also by Korea Electric Power Corporation.

NOMENCLATURE

A_c : counted area of sorbent in the cross-section
A_t : counted total area of the cross-section
S_ϕ : source term
u : velocity of x direction [m/s]
v : velocity of y direction [m/s]
V_f : volume fraction of sorbent the cross-section
w : velocity of z direction [m/s]
Γ_f : turbulent diffusion coefficient [kg/m·s]
ε : turbulent kinetic energy dissipation rate
κ : turbulent kinetic energy [m^2/s^2]
μ : dynamic viscosity [kg/m·s]
μ_{eff} : effective viscosity [kg/m·s]
ρ : density [kg/m^3]
ϕ : general dependent variables

REFERENCES

1. P. S. Nolan, Coal-Tech 2000 International Conference, Jakarta, Indonesia (2000).
2. S. W. Kang, S. C. Oh, H. P. Lee, H. T. Kim and K. O. Yoo, *Korean Chem. Eng. Res.*, **37**(2), 250 (1999).
3. F. J. Collado, *Environmental Progress*, **22**(3), 189 (2003).
4. N. J. Cooper and P. Merati, 43rd AIAA Aerospace Sciences Meeting and Exhibit, Reno, Nevada (2005).
5. A. Thakker and T. S. Dhanasekaran, *Renew. Energy*, **30**, 1359 (2005).
6. A. K. Slone, T. N. Croft, A. J. Williams and M. Cross, *Advances in Engineering Software*, **38**, 244 (2007).
7. C. Y. Park, Y. C. Lee, S. H. Chung and E. S. Sohn, *Korean J. Chem. Eng.*, **7**, 296 (1990).
8. F. Mckenty, L. Gravel and R. Camarero, *Korean J. Chem. Eng.*, **16**, 482 (1999).
9. A. Garea, J. R. Viguri and A. Irabien, *Chem. Eng. Sci.*, **52**(5), 715 (1997).
10. C. Bhasker, *Advances in Engineering Software*, **33**, 71 (2002)
11. J. D. Chung, J. W. Kim, B. H. Kim and Y. M. Park, *J. of KSEE*, **29**(1), 47 (2007).
12. Fluent 6.2 User's Guide.
13. S. V. Patanker, McGraw-Hill (1980).